

CHAPTER 44

MATHEMATICAL SIMULATION OF BOTTOM SEDIMENT MOTION BY WAVES

J.W. Kamphuis
Hydraulics Section
National Research Council
Ottawa, Canada

ABSTRACT

A mathematical model is developed to calculate the amount of bottom sediment moved by wave action. The simplified case of a horizontal bottom and spherical material of uniform size is presented here; however, with some further groundwork it is thought that the model may be extended to actual field conditions without too much difficulty.

INTRODUCTION

In the process of sediment movement in coastal areas the onshore-offshore movement of material by direct wave action plays an important role. An attempt is made in this paper to simulate mathematically the simplified case of movement of bottom sediment of more or less uniform size over a horizontal bottom by wave action. A mathematical model is formulated and calibrated against experimental evidence to afford a better understanding of the physical processes involved. It may be seen that a promising simulation is brought about between mathematical and experimental models and that it will be possible to extend this simulation to field conditions, once further ground work is done in the area of turbulent, oscillatory boundary layer velocities.

By definition it is understood that the term mathematical model, as used in this paper, refers to the system of mathematical equations and assumptions which, when operated on by logically developed computer programming steps and modified by experimental evidence, describes, as completely and accurately as possible, the transport of bottom sediment by wave action.

The parameters are defined as they first appear in the text and a complete notation appears in the appendix. A more detailed explanation of the work done may be found in an earlier publication - Kamphuis (1966), and further papers closely related to this subject are, among others, Vincent (1958), Ishihara, Sawaragi and Amano (1959), Ishihara and Sawaragi (1962), Eagleson and Dean (1961), Eagleson, Glenne and Dracup (1963) and Kalkanis (1964).

DESCRIPTION OF THE MATHEMATICAL MODEL

BOTTOM CONDITIONS

The bottom conditions which are rather random in nature have been assumed to be as in Figure 1. The bottom is assumed to be horizontal and consisting of spherical particles of uniform size. The particles marked 1 to 8 can be displaced from their places without previous removal of other bottom particles. The number of these particles per unit area has been called η , and it may be obtained experimentally simply by counting, with or without optical aids. It was assumed that only these particles participated in the sediment transport i.e. the number of particles from the lower layers exhibiting a net movement was assumed to be balanced, on the average, by the number of particles from the top layer not displaced from their positions. Experimental observations substantiated the validity of this assumption.

WAVE MOTION

Outside Boundary Layer - The wave motion outside of the boundary layer was assumed to be adequately represented by second order of approximation finite-amplitude wave theory. This results in the well-known expression for the water particle velocity outside the boundary layer:

$$u_{\infty} = \frac{\pi H}{T \sinh kd} \cos(\omega t - kx) + \frac{3}{4} \frac{\pi^2 H^2}{L T \sinh^4 kd} \cos 2(\omega t - kx) \quad (1)$$

where

- u_{∞} = horizontal component of the water particle velocity just outside the boundary layer
- d = depth of water
- x = horizontal distance away from the x origin
- t = time
- H = wave height
- T = wave period
- L = wave length
- k = wave number = $\frac{2\pi}{L}$
- ω = wave angular frequency = $\frac{2\pi}{T}$

Second-order wave theory was used since it gives rise to mass transport (asymmetry in u_{∞} was about 25% in some cases). In addition the third order of approximation adds very little to the accuracy, if any, and the measured wave profiles agreed closely to profiles calculated by second-order theory.

Within the boundary layer - The description of the water particle motion within the boundary layer is much more difficult. From observations it was evident that the boundary layer was turbulent when bottom movement occurred. This agrees with Vincent (1958). However, this means immediately that the calculated boundary layer velocities are of an empirical nature. In order to obtain values of this boundary layer velocity which were as realistic as possible, the approach and experimental evidence as described by Kalkanis (1964) was used. This was the most recent available and, although the technique used neglected convective accelerations, the results were found to be reasonable. The theoretical development of Kalkanis was extended in this study to take into account second-order effects. Kalkanis has shown that, from experimental evidence, the following empirical relationship may be postulated for the mean turbulent velocity of water particles anywhere within the boundary layer.

$$\bar{u}_{x,y,t} = \frac{\pi H}{T \sinh kd} \left[\cos(\omega t - kx) - f_1(y) \cos\{\omega t - kx - f_2(y)\} \right] \quad (2)$$

This expression is similar to the one that may be derived theoretically for the laminar boundary layer case except β has been replaced by $f_1(y)$ and $f_2(y)$.

$$\begin{aligned} f_1(y) &= \frac{1}{2} e^{-\frac{267}{R_B}(\beta y)} \\ f_2(y) &= \frac{1}{2} (\beta y)^{2/3} \end{aligned} \quad (3)$$

where $R_B = \hat{u}_\infty D / \nu$, ν being the kinematic viscosity of water and \hat{u}_∞ the maximum value of equation (1). Equations (2) and (3) correspond to small amplitude wave theory. If it is assumed that the second term of equation (1) is superposed upon the first one and has only one half its period then an equivalent second-order expression may be written as:

$$\begin{aligned} \bar{u}_{(x,y,t)} &= \frac{\pi H}{T \sinh kd} \left[\cos(\omega t - kx) - \frac{1}{2} f_5(y) \cos\{\omega t - kx - f_2(y)\} \right] \\ &+ \frac{3}{4} \frac{\pi^2 H^2}{L T \sinh^4 kd} \left[\cos 2(\omega t - kx) \right. \\ &\left. - \frac{1}{2} f_5(y) \cos 2\left\{\omega t - kx - \frac{1}{\sqrt{4}} f_2(y)\right\} \right] \end{aligned} \quad (4)$$

$$\begin{aligned} \text{where} \quad f_5(y) &= e^{-\frac{267}{R_B}(\beta y)} \\ f_2(y) &= \frac{1}{2} (\beta y)^{2/3} \end{aligned}$$

$$R_B = \frac{\hat{u}_\infty D}{\nu}$$

$$\hat{u}_\infty = \frac{\pi H}{T \sinh kd} + \frac{3}{4} \frac{\pi^2 H^2}{LT \sinh^4 kd} \quad (5)$$

Effective Water Velocity - In order to obtain an effective water velocity acting on a particle the integration with respect to y

$$u_w = \frac{1}{Z_2 - Z_1} \int_{Z_1}^{Z_2} \bar{u} \, dy \quad (6)$$

has to be performed. The integration limits are nebulous. Einstein and El-Samni (1949) indicate that:

$$Z_1 = 0.2 D \quad Z_2 = 1.2 D$$

where D is the particle diameter. However, it is easy to see that these are a function of the packing density of the particles in the top layer. For the mathematical model

$$Z_1 = 0$$

$$Z_2 = (0.5 + 0.5 \eta' / \eta) D \quad (7)$$

were used where η' is the number of particles per unit area actually moving at the time of the evaluation of the effective velocity. The integration is complicated further by a number of facts. First, the exposed area of a particle and the boundary layer velocity both vary with y . To include this change of exposed area with y in the integration was found to be too time consuming. Furthermore, as a larger number of particles begin motion, the moving particles interfere with the position of the theoretical bottom as well as with the velocity distribution. Since one can only guess at this additional effect it has also been neglected, and the line of action of u_w has been assumed to be located at the particle centre, its value being determined simply by (6) and (7). The integration may be performed by numerical methods to any desired accuracy. However, since for the mathematical model several thousands of these calculations are performed per set of results, even the crudest integration technique (for instance, the trapezoidal rule using six increments) was found to be much too time consuming and a direct integration method had to be developed.

The method consists of an approximate integration of (4). It may be shown that the expression

$$\left[\omega t - kx - \frac{1}{2} (\beta y)^{2/3} \right]$$

as found by Kalkanis may be represented by two expressions:

$$\begin{aligned} (\omega t - kx - 0.4 - 0.2\beta y) & \quad \beta y \geq 2 \\ (\omega t - kx - 0.4\beta y) & \quad \beta y \leq 2 \end{aligned}$$

over the range of interest. Integration with respect to y of equation (4) then results in:

$$\begin{aligned} u_w = & \frac{1}{Z_2 - Z_1} \left((A + F) (Z_2 - Z_1) \right. \\ & + \frac{BE^2}{C^2 + E^2} \left[e^{-Z_2 C} \left\{ \frac{1}{E} \sin(P - Z_2 E) + \frac{C}{E^2} \cos(P - Z_2 E) \right\} \right. \\ & - e^{-Z_1 C} \left\{ \frac{1}{E} \sin(P - Z_1 E) + \frac{C}{E^2} \cos(P - Z_1 E) \right\} \left. \right] \\ & + \frac{GL^2}{H^2 + L^2} \left[e^{-Z_2 H} \left\{ \frac{1}{L} \sin(K - Z_2 L) + \frac{H}{L^2} \cos(K - Z_2 L) \right\} \right. \\ & \left. - e^{-Z_1 H} \left\{ \frac{1}{L} \sin(K - Z_1 L) + \frac{H}{L^2} \cos(K - Z_1 L) \right\} \right] \quad (8) \end{aligned}$$

where D has its usual meaning of particle diameter and

$$\begin{aligned} B &= \frac{1}{2} \frac{\pi H}{T \sinh kd} & A &= 2B \cos(\omega t - kx) \\ C &= \frac{267\beta}{R_B} & H &= C^{0.707} \\ G &= \frac{3}{8} \frac{\pi^2 H^2}{LT \sinh^4 kd} & F &= 2G \cos 2(\omega t - kx) \end{aligned}$$

For $\beta y \leq 2$: $P = (\omega t - kx)$, $K = 2P$, $E = 0.4\beta$ and $L = 0.5\beta$.

For $\beta y \geq 2$: $P = \omega t - kx - 0.4$, $K = 2\omega t - 2kx - 0.8$, $E = 0.2\beta$ and $L = 0.25\beta$.

A comparison between (8) and the numerical integration by trapezoidal rule with one hundred increments indicates close agreement, thus justifying the approximations made in the integration procedure.

PHYSICAL PROPERTIES

In the mathematical model variations in the physical properties of the water were neglected with the exception of the variations in temperature (viscosity). The properties of the bottom material taken into account were the relative underwater density $\rho' = (\rho_s - \rho_w) / \rho_w$ the representative particle diameter, D, and the angle of internal friction ϕ . For the materials used in the experimental phase of the study, these properties are given in Table 1:

TABLE 1
DESCRIPTION OF THE MATERIALS

		ρ'	D	ϕ
Material	Shape		mm	deg
Cellulose Acetate	Sphere	0.30	3.68	26
Nylon	Parallelepiped	0.133	4.00	35
Sand	Grain	1.65	0.4	34
Magnetite ore	Grain	3.35	0.18	34

ρ' was obtained by weighing batches of material in air and submerged in water. D was obtained by actual measurement, by fall velocity tests and by the weighing of a number of the particles; it was assumed that the representative particle diameter was the diameter of a sphere of equal volume. ϕ was determined in several ways. Firstly, a constant displacement direct shear test was performed. Subsequently, particles were glued to a strip of aluminum. This roughened strip was then tilted under water, with some loose particles placed on it and the angle at which the loose particles began to move was observed. Finally, a bed of loose particles, restrained at the ends was tilted under water and movement observed. Using the first method, the results were not too accurate for the larger particles, since considerable arching took place in the regular size 6 x 6 cm shear box, resulting in too high a value for ϕ . Since in addition the other two methods were rather subjective, the observed values of ϕ are expected to be rather doubtful.

PARTICLE MOTION

The process of sediment movement has been subdivided into two stages: Initial Motion and Established Motion.

Initial Motion - The Initial Motion Condition may be derived by equating moments about point O (Figure 2). The

drag force, F_D , is the total drag, a combination of surface drag and form drag. The moment arm of this force is therefore difficult to determine. Chepil (1959) found that the line of action of the drag force was about $0.3 D$ below the top of the particles when testing soil particles of 3.36 to 6.4 mm diameter in a turbulent boundary layer of about 30 cm thickness. In the case of the cellulose acetate material of diameter $D = 3.68$ mm, a boundary layer thickness of about 4 mm was noted; this is quite unlike the tests performed by Chepil. However, since Chepil found the position of the line of action to be relatively constant throughout his tests, this position was accepted for the mathematical model. The actual moment arm of the drag force could well be quite different due to another ratio of surface drag to form drag. The line of action of the added mass force, F_A , is assumed to be $D/2$, the average value during the equation process of initiation of motion. The following equation of moments may now be written about point O.

$$\begin{aligned} \sum M_O = & F_D \frac{D}{2} (0.4 + \cos \phi) + F_L \frac{D}{2} \sin \phi \\ & + F_A \frac{D}{2} + F_p \frac{D}{2} \cos \phi \\ & - F_w \frac{D}{2} \sin \phi = 0 \end{aligned} \quad (9)$$

where F_D , F_L , F_p and F_w are the forces due to drag, lift added mass, pressure and weight respectively

$$\begin{aligned} F_w &= \rho_w \frac{\pi D^3}{6} \rho' g \\ F_L &= I C_L \rho_w \frac{\pi D^2}{8} (u_w - u_s)^2 \\ F_D &= I C_D \rho_w \frac{\pi D^2}{8} (u_w - u_s) |u_w - u_s| \\ F_A &= C_A \rho_w \frac{\pi D^3}{6} \left[\frac{du_w}{dt} - \frac{du_s}{dt} \right] \\ F_p &= \rho_w \frac{\pi D^3}{6} \frac{du_w}{dt} \end{aligned} \quad (9a)$$

F_R = Reaction force which causes no moment about point O.

ρ_w = density of water

g = acceleration due to gravity

u_s = sediment particle velocity

$I C_D$ = coefficient of drag for initial motion

$I C_L$ = coefficient of lift for initial motion

C_A = coefficient of added mass

Equation (9) may be rewritten as:

$$0.75 [I C_D (0.4 + \cos \phi) + I C_L \sin \phi] u_w^2 \times \frac{1}{D} + C_A \frac{du_w}{dt} + \cos \phi \frac{du_w}{dt} = \rho' g \sin \phi \quad (10)$$

and this equation, with some slight modifications to take into account the directions of the accelerations, becomes:

$$\bar{D}_C = \frac{0.75 [I C_D (0.4 + \cos \phi) + I C_L \sin \phi] u_w^2}{\rho' g \sin \phi - C_A \frac{u_w}{|u_w|} \frac{du_w}{dt} - \cos \phi \frac{u_\infty}{|u_\infty|} \frac{du_\infty}{dt}} \quad (11)$$

where \bar{D}_C is the mean critical diameter (the diameter that will just be moved on the average). This equation will be referred to as the Initial Motion Condition.

The use of $\frac{du}{dt}$ rather than $\frac{\partial u}{\partial t}$ is justified since the model takes the variation of u with x and y into account by performing an integration with respect to y to obtain u_w and a step integration with respect to x described in the following section.

This initial motion condition is obviously subject to severe limitations. It is assumed that the particle is subjected to the undisturbed velocity conditions, whereas, in actual fact, neighbouring particles give rise to wake interference patterns, sheltering etc. The vertical components of velocity due to percolation have also been neglected. Equation (11) also is a quotient, the denominator of which consists of a difference, making the value of \bar{D}_C very sensitive to slight changes in ϕ , C_A and ρ' .

In addition, it is evident that the initial motion condition only gives average values and that for instance, when \bar{D}_C becomes greater than D , not all particles suddenly begin motion simultaneously. This necessitates the derivation of an Initial Motion Distribution Function. It may be assumed that:

$$D_C = \bar{D}_C + D'_C \quad (12)$$

where the fluctuations in D_C are caused by a combination of turbulent fluctuations and local variations in ϕ , packing and sheltering. It is usually assumed that this distribution is normal, however, figure 3 indicates that if the standard deviation of the distribution is greater than $\bar{D}_C/3$ (the mathematical model indicated this to be the case) the distribution becomes meaningless due to a tail of negative diameters. The calibration of the mathematical model indicated that a Rayleigh distribution with \bar{D}_C as the most probable diameter gave the best results.

$$P = e^{-\frac{1}{2} \left[\frac{D}{\bar{D}_C} \right]^2} \quad (13)$$

Established Motion - Once the conditions for initial motion have been satisfied, the particle is assumed to become subject to Established Motion Conditions. From preliminary observations it may be postulated that the motion of the particles is mainly by rolling and therefore the following force equation may be written:

$$\sum F = m_s a_s \quad (14)$$

$$F_p + F_A + F_D - F_\epsilon = m_s a_s \quad (15)$$

where F_ϵ is the force caused by rolling friction.

$$F_\epsilon = \epsilon \frac{u_s}{|u_s|} [F_W - F_L] \quad (16)$$

and ϵ is a coefficient of rolling friction. From equations (15), (16) and (9a) it may then be shown, writing the differentials as differences, that:

$$\begin{aligned} \Delta u_s = & \frac{1}{C_1} (\Delta u_{\infty} + C_A \Delta u_w) + C_2 [(u_w - u_s) |u_w - u_s|] \Delta t \\ & + C_3 [(u_w - u_s)^2 \frac{u_s}{|u_s|}] \Delta t - C_4 \left[\frac{u_s}{|u_s|} \right] \Delta t \end{aligned} \quad (17)$$

where

$$\begin{aligned} C_1 = & \frac{\rho_s}{\rho_w} + C_A & C_2 = & \frac{3}{4} \epsilon C_D / C_1 D \\ C_3 = & \frac{3}{4} \epsilon C_L \epsilon / C_1 D & C_4 = & \rho' g \epsilon / C_1 \end{aligned} \quad (18)$$

This is known as the Established Motion Condition. ϵC_D and ϵC_L are the drag and lift coefficients for established motion and ρ_s is the sediment density. The established motion condition is an implicit function in u_s and must be solved by iteration. Normal iteration procedures, however, could converge, diverge or oscillate, depending on the initially assumed value of u_s and it was necessary to develop a special iterative procedure to deal with this problem - Kamphuis (1966).

Coefficients - The hydrodynamic coefficients C_D , C_L , C_A and ϵ have been subject to a great deal of discussion in literature and it is hoped that some of the uncertainty of the values of these coefficients has been removed by this mathematical model. Added mass has been discussed among others by Landweber (1961), Stelson (1955), Eagleson and Dean (1961), Streeter (1948), O'Brien and Morrison (1952) and recently by Odar (1964). These studies indicate:

$$0.5 \leq C_A \leq 1.59$$

and therefore a definite need is shown for further research in this area. The assumption that C_A is constant is an obvious over simplification. Odar (1964) derives an expression where C_A varies with a so-called acceleration number, however, when this relationship was incorporated in the model, curious results were obtained, indicating that perhaps this relationship is also over-simplified. Therefore, the assumption that C_A is constant throughout the wave cycle was made for the final calibration steps of the mathematical model. Drag and lift coefficients have also been subject of much discussion e.g. McNown (1951), Carty (1957), Eagleson and Dean (1961) and Chepil (1958), (1959), (1961). Experimental work by the

author indicated that Carty's value for C_D was reasonable and could be incorporated in the model as E^{CD} . Additional tests indicated that E^{CL} should be assumed equal to $E^{CD}/2$. Although Chepil (1958) found the constant value $I^{CD} = 0.08$, it was assumed for the mathematical model that $I^{CD} = C_I \times E^{CD}$ where C_I varies with R and represents the combined effect of sheltering, wake interference and boundary proximity. The relationship $I^{CL} = 0.85 I^{CD}$ as found by Chepil (1958) was used, however. An expression for the rolling friction coefficient, ϵ , was obtained by equating forces as shown in Figure 4. This leads to the relationship:

$$\epsilon = \frac{\rho' g D \sin \alpha - 0.75 E^{CD} u_s^2}{\rho' g D - 0.75 E^{CL} u_s^2} \quad (19)$$

Experimentally for the cellulose acetate $0.55 \leq \epsilon \leq 0.58$ and for the nylon $\epsilon \approx 0.8$ were found by observing several values of x and steady state rolling velocities simultaneously for these materials.

LOGIC OF THE MATHEMATICAL MODEL

The model evaluates the function:

$$G = f(H, T, d, t, \rho_s, D, \eta, \phi, C_A, C_D, C_L, \epsilon) \quad (20)$$

where G_M is the solid discharge value calculated mathematically. The wave period is divided into n time increments, each of length Δt . The origin of time for this calculation has been taken as the time when $u_w = 0$, going from the negative direction (with respect to the direction of wave propagation) to the positive direction, giving rise to a phase angle of approximately 270° with the time origin of equations (1) through (5) and (8). At times $t = 0$ and $t = \Delta t$ a water particle velocity is calculated using (8) and a mean velocity u_w during the first time increment is obtained. Now from the initial motion condition (11) and equation (13), η' , the number of particles per unit area set into motion during this first time increment, may be calculated using the formula:

$${}_k \eta' = (P_k - P_{k-1}) \eta \quad (21)$$

From the established motion condition, the change in velocity of the solid particles during Δt may be computed and also a mean value \bar{u}_s for the time increment. At this point a second iteration procedure is necessary. The distance travelled by the particles moved in the first time increment must be taken into account and a new value of u_w at $t = \Delta t$ is calculated, resulting in a second approximation of \bar{u}_s and so on until the required accuracy is reached. It is now possible to obtain an incremental value for the solid discharge, $\Delta G_M(1,1)$, in weight per unit width.

$$\Delta G_M(k,i) = \rho_s g {}_k \eta' \frac{\pi D^3}{6} \bar{u}_s(k,i) \Delta t \quad (22)$$

The bracketed figures (k,i) indicate respectively the number of the time increment, during which the set of particles

under consideration began to move, and the time increment for which the calculation is performed. Calculations for the first time increment are now completed and the calculations of the second time increment may be commenced. Once again for this time increment $\bar{u}_w(2,2)$ may be calculated using (8) and $z\eta'$ using (11), (13) and (21). The established motion condition (17) will give $\bar{u}_s(2,2)$ and, after an iteration to obtain the proper value of \bar{u}_s , $\Delta G_M(2,2)$ may be computed using (22). Next the solid discharge $\Delta G_M(1,2)$, attributed to the particles that began motion in the previous time increment, must be computed. u_w must be calculated at $t=\Delta t$ for these particles now at position $x(1,1)$ and by iteration for $t=2\Delta t$. Using (22) $\Delta G_M(1,2)$ may be computed, completing the calculations for the second time increment. Similarly for the next time increment $\Delta G_M(1,3)$, $\Delta G_M(2,3)$ and $\Delta G_M(3,3)$ may be computed. There comes a time, however, $t=m\Delta t$ when no further particles are set into motion. At this time it was assumed that all moving particles could be represented by $\hat{\eta}_M$ the maximum (total) number of particles per unit area travelling in the direction of wave propagation at a weighted velocity $\bar{u}_s(m,m)$ and located at a weighted distance $x(m,m)$ from the origin. This step effected a total reduction of the required computing time by 75% and could be made because preliminary computer analysis indicated that all particles reached approximately the same velocity about three time increments after being set into motion and stopped movement within one or two time increments of each other. Subsequent analysis indicated that the values of solid discharge calculated by the shorter procedure differed by no more than 5% from the values obtained by the proper procedure. Using these aggregate quantities $\hat{\eta}_M$, $\bar{u}_s(m,m)$ and $x(m,m)$, further estimates of ΔG_M may be obtained using (22), until such time that all solid particles come to rest. Subsequent to this, with the negative water velocities present, the identical procedure as described above for the positive water velocities is followed to obtain ΔG_M values for the second half-cycle. Once this is completed, the incremental sediment discharge values are summed over a wave period T and the total solid discharge in weight of sediment per unit width per minute may be computed.

$$G_M = \frac{60}{T} \sum_{k=1}^n \sum_{i=1}^n \Delta G_M(k,i) \quad (23)$$

When the calculation is now carried on for subsequent cycles, other values of G_M for those cycles could be obtained; however, the difference was small between cycles, as long as calculations were started at the time origin mentioned previously. This is a rather simplified explanation of the logic involved

in the calculation of solid discharge. Many contingencies have arisen during the calculation, each of which had to be met with corrective logical steps, but these have been omitted for clarity.

EXPERIMENTAL WORK

To obtain the experimental results with which the mathematical model was calibrated, a concrete wave flume 2 feet wide, 4 feet deep and 100 feet long was built (Figure 5). Details of the test section designed to collect the bottom material and obtain a value of G_E are shown in Figure 6. To begin each test the bed was tamped lightly and levelled. The wave generator was then started and steady conditions set up. When these steady conditions were thought to exist the removable trap was lowered into position without noticeable disturbance to the water-and sediment motion and the collection of material begun. For each test H , T , d , wave surface profile, water temperature, mass transport curve and the boundary layer details were determined, the last two very roughly. G_E was obtained by weighing the material collected in the trap over a period of time and η_E' was observed through a simple sighting apparatus since photographic methods were useless due to a lack of contrast between exposures of moving particles and still particles. The materials previously described were used in these tests and for further details of the experimental method the reader is referred to Kamphuis (1966). It was seen that the finer materials - sand and magnetite produced rippled beds, whereas the beds of the larger materials - cellulose acetate and nylon - remained sensibly plain. The larger materials were used for calibration. This is justified since the model ripples are not to scale. These ripples are of the order of one orbital diameter, whereas the ripples occurring in the field are only a fraction of an orbital diameter long in general. Therefore, a particle in the model may move along the upwave crest of one ripple, be caught in an eddy which forms behind this ripple and so remain suspended until the water particle velocity has reversed. The negative velocity will then deposit this suspended sediment particle one, perhaps even two ripple crests back, causing possibly a negative transport of sediment (with respect to the direction of wave propagation). In the field, the velocity in the positive direction may advance the particle a number of ripple lengths to be returned one or two ripple lengths, causing, in general, a positive transport of sediment. In addition to this, the comparatively rougher model bottom reduces the asymmetry of the bottom water particle velocities introducing a further error. Thus the model tests with rippled beds are not very useful when simulating field conditions, a phenomenon recognized by Russel and Dyke (1963), Inman and Bagnold (1963) and others.

RESULTS

The calibration of the mathematical model was as follows. The best estimates of all the parameters of equation (20) were inserted in the mathematical model and G_M calculated for 25 to 40 different conditions of wave motion. The values of G_M were then plotted against those of G_E , the experimental values of the solid discharge for identical wave and particle parameters and with the use of this plot (G_M vs G_E) and two additional plots, $\hat{\eta}'_M$ vs $\hat{\eta}'_E$, the maximum number of particles per unit area moving in the direction of wave propagation, and $\hat{P}_E = \hat{\eta}'_E / \eta$ against D/\bar{D}_c , a representation of the proper initial motion distribution function, the hydrodynamical parameters were adjusted, and further calibrations were made until the best possible solution was obtained. This method was rather subjective but it was the only way to obtain a properly calibrated model. Normal statistical methods, although used to some extent, could not easily be justified since these assume normal distributions and variables that are totally independent. Figures 7, 8, 9, 10, 11, 12 demonstrate the relationships for two sets of hydrodynamic parameters. It must be kept in mind that each point shown on these plots is subject to two types of error: the experimental error in G_E and the inherent mathematical error due to assumptions, truncations etc. in G_M . Thus each point represents a rectangular field of values and could be located anywhere within this error field.

Because of the errors in both G_M and G_E the calibration was a tedious and lengthy procedure. In total 70 sets of parameters were tested. For the cellulose acetate it appeared that $\phi = 26^\circ$, $C_A = 0.6-0.7$ and $C_I = 1/14-1/15$ gave the best results, using E^{CD} as postulated by Carty (1957) and Eagleson and Dean (1961). The value of ϕ is as one would expect theoretically, C_A is slightly greater than the theoretical value of 0.5 due to the proximity of the boundary, and C_I is, as one would expect, since at large values of R , $1.2 \geq E^{CD} \geq 1.0$ and so $0.083 \geq I^{CD} = C_I \times E^{CD} \geq 0.07$, which is close to the constant value obtained by Chepil (1958). In addition η was found to be 5000 particles /ft², a value that was obtained by simply counting the number of moveable particles and ϵ was found to be the same as observed by the simple experiment described earlier.

In the final analysis, however, no amount of regrouping and re-evaluation of the parameters could reduce the scatter in the results indicated in the figures. The contours of constant values of r in figure 10 show that there is a definite relation between the scatter in the results and the value of r , the assymetry of the water particle velocity just outside the boundary layer. This would seem to indicate that the effective water velocity, being related to r and being the very important prime mover in this study, could be wrong.

This is quite possible since the calculation is based on a single empirical study, one of the very few in this field, and since several difficulties involved in evaluating u_w by equation (6) have been circumvented by simplifying assumptions.

The mathematical model was subsequently verified by comparing it to the experimental results obtained for the nylon and to experimental results obtained by Vincent (1958) using pumice, (Figures 13 and 14). The results are quite promising. The mode of movement of the nylon was quite different from the cellulose acetate. The nylon had a tendency to move en masse, almost like a thick suspension for the larger values of G_E . This may be seen in Figure 13 where, for high values of G_E , the predicted G_M is much too low. It was considered however, that the cellulose acetate represented the motion in the field more closely than the nylon. For the pumice, considering the fact that ϕ , η and ϵ were estimated without having seen the material, the results also looked promising. Once again, the hydrodynamic coefficients are as one would expect theoretically or empirically.

CONCLUSIONS

From the work done it may be concluded that:

1. A mathematical model may be constructed to simulate bottom sediment movement under waves along the lines of this paper. This model will necessarily be subject to much empiricism. Because of the large number of calculations made, each with its own errors, it is to be expected that the accuracy of the results is not very high. This study has shown however, that the accuracy is considerably better than a classical error study would tend to indicate.
2. When one enters the observed water and bottom sediment parameters (H , T , d , ρ_s , D , η and ϕ) and the semi-empirical or theoretical values of C_A , E^{CD} , C_I , E^{CL} , I^{CL} , and ϵ , the hydrodynamic parameters, one may expect a fairly close prediction of the actual sediment discharge resulting from an experimental model, i.e. the mathematical model simulates an experimental model reasonably close, even for particles that are far from spherical and for which the particle parameters ϕ , η , ϵ and have been estimated instead of determined experimentally.
3. In any study of sediment motion a substantial scatter is to be expected due to the inherently statistical nature of the whole problem. - Kamphuis (1966). It is thought, however, that in this study also a large proportion of the scatter may be due to an inadequate knowledge about velocities in the boundary layer and perhaps due to too many simplifying assumptions in the evaluation of the effective water velocity, the prime moving force. Until further research is performed

in this area, it is of little value to extend the mathematical model to include bottom slope, ripple formation, etc, which is mathematically not too difficult. Thus the simulation of field conditions, although mathematically quite feasible, is, at present, beyond our reach until the hydrodynamics of the boundary layer becomes more clear.

ACKNOWLEDGMENTS

This study was performed at the hydraulics laboratories and computation centre of Queen's University, Kingston, Canada. The author gratefully acknowledges the assistance and encouragement given by Dr. A. Brebner, Head of the Civil Engineering Department and also wishes to thank the National Research Council of Canada for the financial assistance received to complete this project.

REFERENCES

- Carty, J.J. (1957). Resistance Coefficients for Spheres on a Plane Boundary: B.S. Thesis, M.I.T.
- Chepil, W.S. (1958). Use of Evenly Spaced Hemispheres to Evaluate Aerodynamic Forces on a Soil Surface: Trans. A.G.U., Vol. 39, p. 397.
- Chepil, W.S. (1959). Equilibrium of Soil Grains at the Threshold of Movement by Wind: Soil Science Society of America Proceedings, 1959, p. 422.
- Chepil, W.S. (1961). The Use of Spheres to Measure Lift and Drag on Wind Eroded Soil Grains: Soil Science Society of America Proceedings, 1961, p. 343.
- Eagleson, P.S. & Dean, R.G. (1961). Wave Induced Motion of Bottom Sediment Particles: Trans. A.S.C.E., Vol. 126, p. 1162.
- Eagleson, P.S., Glenne, G. and Dracup, J.A. (1963). Equilibrium Characteristics of Sand Beaches: Journal of Hydraulics Division, A.S.C.E., Vol. 89, No. 1, p. 35.
- Einstein, H.A. and El-Samni, A. (1949). Hydrodynamic Forces on a Rough Wall: Review of Modern Physics, Vol. 21, No. 3, p. 520.
- Inman, D.L. and Bagnold, R.A. (1963). The Sea, M.N. Hill, Editor, Interscience Publishers, Vol. 3, p. 529.

- Ishihara, T., Sawaragi, T., and Amano, T. (1959).
Fundamental Studies on the Dynamics of Sand
Drifts: Reports 1 and 2, Coastal Engineering
in Japan, Vol. II, p. 35.
- Ishihara, T. and Sawaragi, T. (1962). Fundamental Studies
on Sand Drifts: Report 3, Coastal Engineering in
Japan, Vol. V, p. 59.
- Kalkanis, G. (1964). Transportation of Bed Material
Due to Wave Action: Coastal Engineering
Research Centre, U.S. Army, Tech. Mem. No. 2.
- Kamphuis, J.W. (1966). A Mathematical Model to Advance
the Understanding of the Factors Involved in the
Movement of Bottom Sediment by Wave Action:
C.E. Research Report, No. 53, Queen's University,
Kingston, Canada.
- Landweber, L. (1961). Handbook of Fluid Dynamics,
V.L. Streeter Editor, McGraw-Hill, Chapter 13,
p. 36.
- McNown, J.S. (1951). Particles in Slow Motion: Houille
Blanche, Vol. 6, p. 701.
- O'Brien, M.P. and Morrison, J.R. (1952). The Forces
Exerted by Waves on Objects: Trans. A.G.U.,
Vol. 33, p. 32.
- Odar, F. (1964). Forces on a Sphere Accelerating in
a Viscous Fluid: Cold Regions Research and
Engineering Laboratory, U.S. Army, Research
Report No. 128.
- Russel, R.C.H. and Dyke, J.R.J. (1963). Net Sediment
Transport Direction - Waves over a Horizontal
Bed: I.A.H.R. (London), p. 41.
- Stelson, T.E. (1955). Virtual Mass and Acceleration
in Fluids: Engineering Mechanics Division,
A.S.C.E., Vol. 81, Sep. 670.
- Streeter, V.L. (1948). Fluid Dynamics, McGraw-Hill, p. 80.
- Vincent, G.E. (1958). Sediment Transport on a Horizontal
Bed due to Wave Action: Coastal Engineering 1958,
p. 326.

APPENDIX

VARIABLES

- a - Acceleration
- C - Coefficient or constant
- D - Representative particle diameter
- d - Depth of water (from the still water level -S.W.L- to the theoretical bottom)
- e - Base of natural logarithm
- F - Force
- f - Function
- G - Solid discharge
- g - Acceleration due to gravity
- H - Wave height
- k - Wave number - $\frac{2\pi}{L}$
- L - Wave length
- M - Moment
- m - Mass
- n - Number of incremental time steps per wave period
- P - Probability
- p - Pressure
- R** - Reynolds number
- r - Assymetry ratio = $\frac{+\hat{u}_{\infty} - \hat{u}_{\infty}}{+\hat{u}_{\infty}}$
- T - Wave period
- t - Time
- u - Horizontal velocity component
- x - Horizontal distance
- y - Vertical distance
- Z - Limit of integration
- ϕ - Angle of inclination
- β - $(\omega / 2\nu)^{1/2}$
- Δ - Incremental value
- ϵ - Relative coefficient of rolling friction
- η - Number of particles / unit area situated in the top layer of bed material that can be displaced immediately
- η' - Number of particles/unit area actually moving
- ν - Kinematic viscosity of water
- ρ - Density
- ρ' - Relative underwater density
- σ - Standard deviation
- ϕ - Natural angle of repose of the bed material or angle of internal friction
- ω - Wave angular frequency

SUBSCRIPTS

- A - Added mass
- B - Bottom
- C - Critical

- D - Drag
- E - Experimental or established
- I - Initial
- L - Lift
- M - Mathematical (i.e. derived by the
mathematical model)
- O - A point O about which moments are taken
- p - Pressure
- R - Reaction
- s - Solid or sediment
- W - Weight
- w - Water
- ϵ - Rolling friction
- ∞ - Just outside the boundary layer
- +
- - In direction opposite to wave propagation

SUPERSCRIPTS

- \wedge - Maximum value
- $\bar{\quad}$ - Mean value

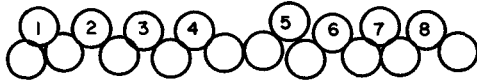


Fig. 1. Assumed bottom conditions.

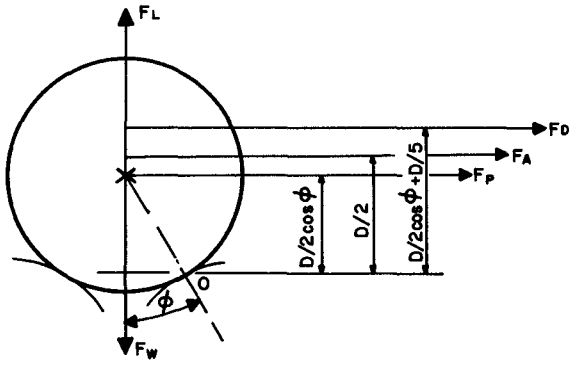


Fig. 2. Diagram of forces.

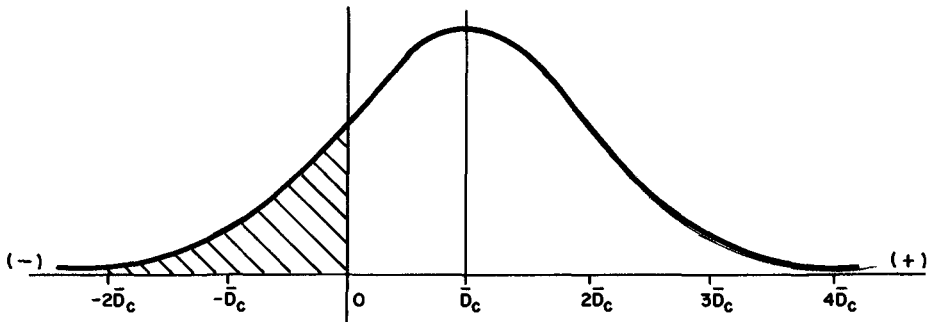


Fig. 3. Normal distribution with $\sigma = \bar{D}_c$.

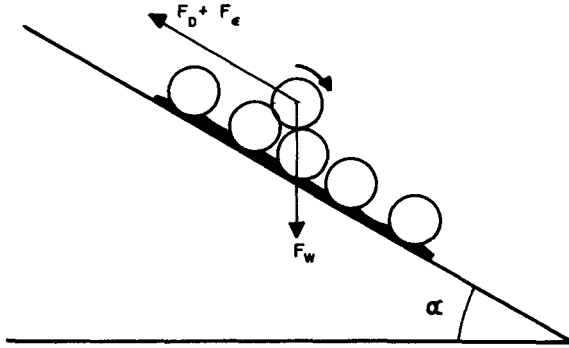


Fig. 4. Force diagram for rolling friction evaluation.

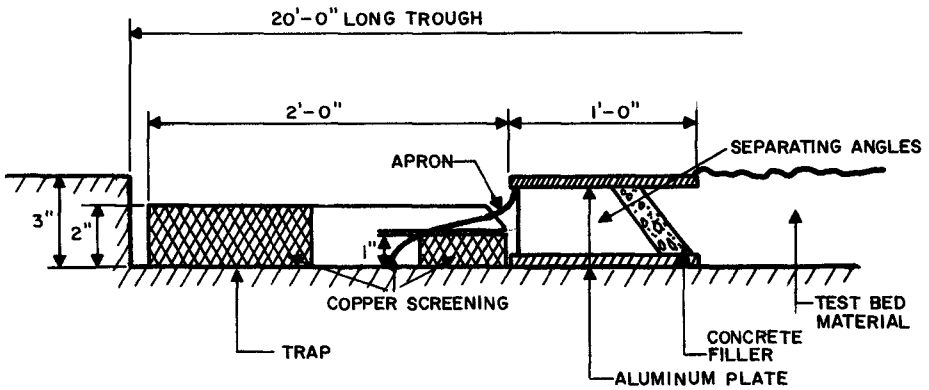


Fig. 6. Test section detail.

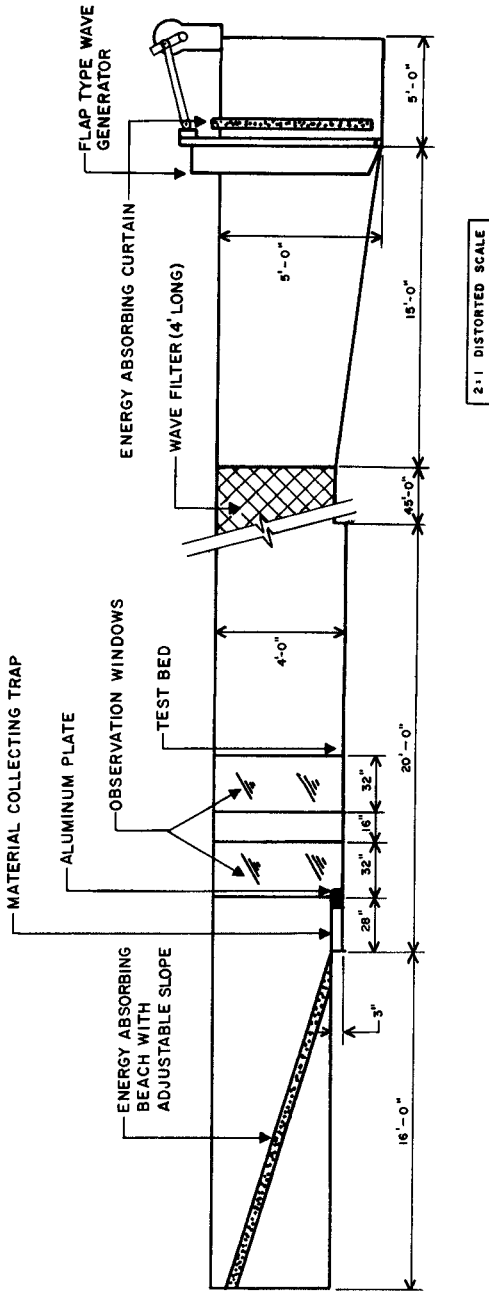


Fig. 5. Experimental wave flume.

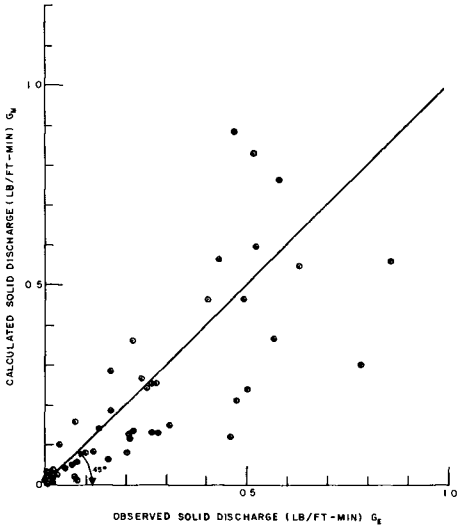


Fig. 7. Calibration curve—solid discharge.

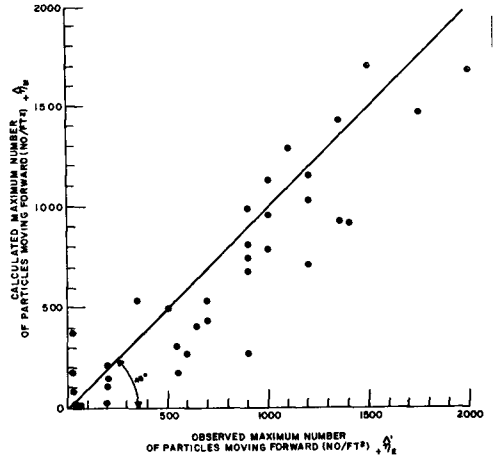


Fig. 8. Calibration curve—particles moving.

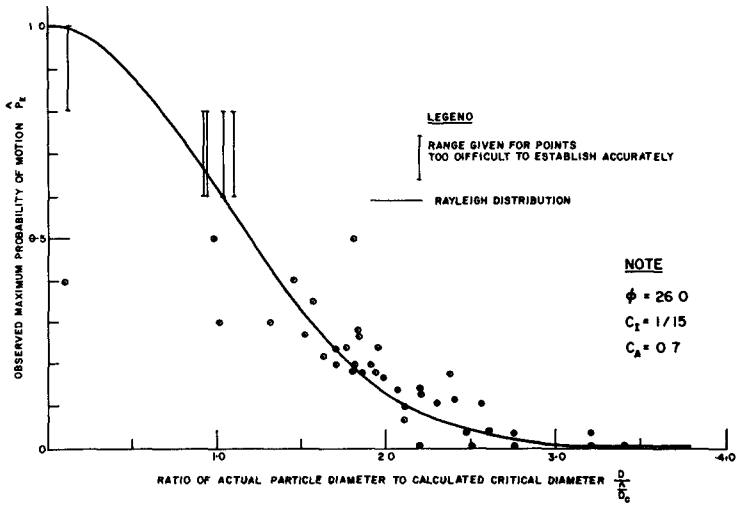


Fig. 9. Observed distribution curve.

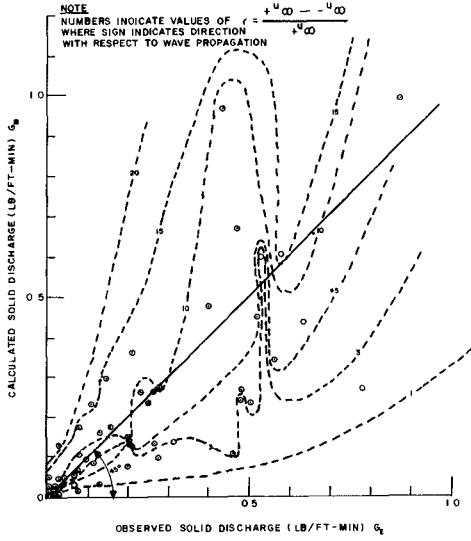


Fig. 10. Calibration curve—solid discharge.

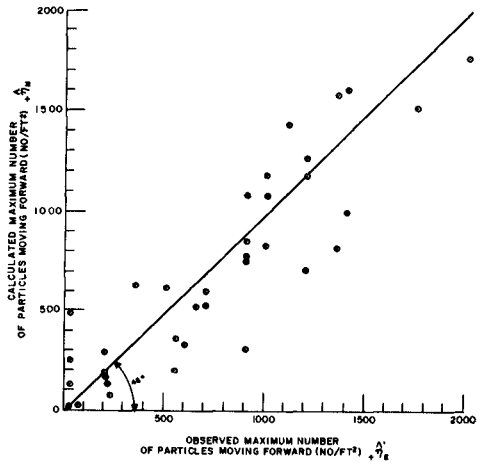


Fig. 11. Calibration curve—particles moving.

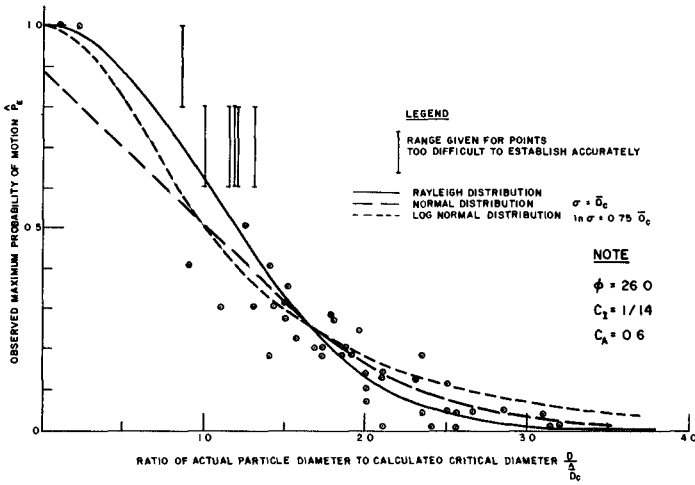


Fig. 12. Observed distribution curve.

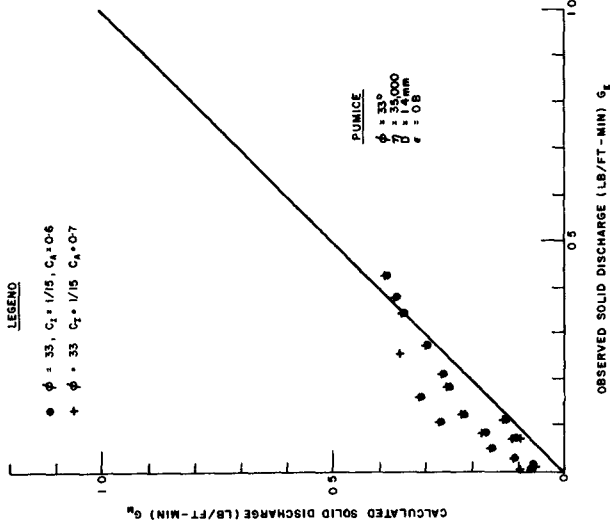


Fig. 14. Verification curve—pumice.

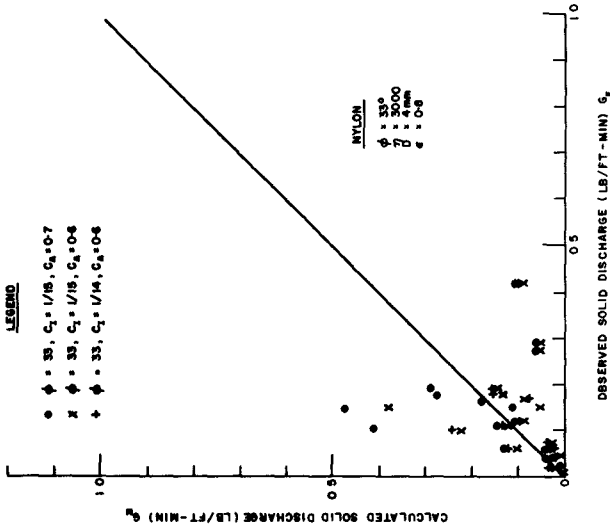


Fig. 13. Verification curve—nylon.

